Chapter

Mechanism of In-Situ Catalytic Cracking of Biomass Tar over Biochar with Multiple Active Sites

Dongdong Feng, Yu Zhang, Yijun Zhao and Shaozeng Sun

Abstract

Biomass tar is the bottleneck in the development of efficient utilization of biomass syngas. The in-situ catalytic cracking biomass tar with multi-active biochar is investigated in a two-stage fluidized bed-fixed bed reactor. It indicates that adding H_2O or CO_2 is found to improve the homogeneous and heterogeneous cracking of biomass tar. Activation of biochar by H_2O or CO_2 impacted the morphology of biochar surface and distribution of metal species. H_2O or CO_2 affects the creation and regeneration of pore structures, influencing the biochar structure and dynamical distribution of alkali and alkaline earth metal species (AAEMs), which ensure enough surface active sites to maintain the catalytic activity of biochar. The tar cracking into low-quality tar or small-molecule gas may be catalyzed by K, while the combination of tar with biochar would be promoted by Ca. The volatilizations of K and Ca, due to their reaction with volatiles, are to a large extent in accordance with their valences and boiling points. The subsequent transformation from the small aromatic ring systems to the larger ones occurs due to the volatile-biochar interaction. During tar cracking over biochar, K and Ca act as the active sites on biochar surface to promote the increase of active intermediates (C–O bonds and C–O–K/Ca).

Keywords: biochar, tar, catalytic cracking, AAEM species

1. Introduction

Tar is a generic term comprising all organic compounds present in syngas except for gaseous hydrocarbons. Tars can condense to more complex structures in pipes, filters, or heat exchangers of downstream equipment and processes, which may cause mechanical breakdown of the entire system [1]. For biomass gasification, the allowable limit for tar in the producer gas is less than 5 mg/Nm^3 for a direct-fired gas turbine [2], and for some fuel synthesis processes, the contents of tar and ammonia are required to be <0.1 mg/Nm^3 and <10 ppm, respectively [3–5], in order to protect the catalysts and downstream equipment and to improve the overall efficiency and economics. The tar mixture is classified into five classes by Padban [6]: undetectable, heterocyclic, light aromatic hydrocarbons (LAHs), light polyaromatic hydrocarbons (LPAHs), and heavy polyaromatic hydrocarbons (HPAHs). The removal of biomass tar is one of the main challenges for the biomass gasification industry [7, 8]. Catalytic cracking is a known method for the efficient removal of biomass tar [9–12]. Biochar, as a product of pyrolysis and gasification of biomass, is a relatively

cheap catalyst with high activity in tar heterogeneous cracking [13–20]. During tar catalytic cracking over biochars, even after the loss of catalytic activity through coking, the biochar samples can still be directly combusted, so as to recover the chemical energy of catalyst, thus avoiding any reprocessing as a result of deactivation.

In addition to the analysis of model tar compounds [21–23], studies of biomass tar over biochar mainly discuss the reforming of real tar from raw materials [24, 25]. However, the AAEM species (e.g., Na, K, Mg, and Ca) in raw biomass play an important role as the "cross points" during tar formation. The chemical bonds between AAEM species and the carbon matrix are repeatedly breaking and reforming. This process promotes the production of gaseous products from the fatty acid tar and a degree of small aromatic compounds. Simultaneously, larger aromatic ring compounds (≥5 aromatic ring system) are formed within the biochar structure [26, 27]. The presence of AAEM species can inhibit the release of volatile matter (especially for biomass tar)—even the strong interaction between volatile materials and biochar will affect tar composition, leading to the catalytic conversion of the real tar components before contacting with the catalyst, which misleads mechanistic studies of subsequent heterogeneous reforming over biochar catalyst.

The formation (e.g., 500–700°C) and thermal decomposition (e.g., 700–900°C) of tar during the gasification process are an extremely complex multistep reaction [28–32], which involves not only homogeneous conversion, but also heterogeneous reforming. H_2O and CO_2 are two important reforming agents [33] in the biomass gasification industry. Studying the influence of H_2O and CO_2 on tar homogeneous transformation and heterogeneous reformation is valuable to better understand the analysis of the tar complex gas-solid phase reaction. However, there is still less research on separate discussion between homogeneous conversion and heterogeneous reforming of biomass tar over biochar. Although there are reports detailing the influence of H_2O and CO_2 on tar during the gasification process [34–39], they were mainly focused on the single concentration of reforming agent (15 vol.% H_2O or pure CO_2 atmosphere). There has yet to be detailed a complete understanding of the influence of H_2O and CO_2 on the homogeneous conversion and heterogeneous reforming over biochar as a function of biomass tar evolution.

The effects of reforming agent concentration and reaction temperature on the tar homogeneous conversion and heterogeneous reforming over biochar were investigated in a two-stage fluidized bed/fixed bed reactor. The H-form biomass samples (with little AAEM species) were used to provide the real tar components, which effectively inhibited the tar-AAEM interactions in gas phase during H_2O/CO_2 homogeneous conversion and prevented any secondary catalytic effects of AAEM species from the volatilization of raw materials on the biochar catalyst surface. The analysis of biochar structures examined with Raman spectroscopy to comprehensively elucidate the changes of biochar catalyst structure after the H_2O and CO_2 heterogeneous reforming of biomass tar. In addition to the measurement of tar yields, GC/MS spectroscopy was used to characterize the detailed structural features of tar [40], so as to understand the molecular biomass tar transformation pathway and the coupling mechanism (e.g., collaboration and interaction effects) between the biochar structure and the AAEM species during tar reforming.

2. Experiment

2.1 Material preparation

Biomass (rice husks) obtained from the Wu Chang area in Harbin, Heilongjiang Province, China, was used in the experiments. The samples were dried overnight

at 105°C, pulverized, and sieved to obtain a fraction with particle sizes between 0.15 and 0.25 mm. The proximate and ultimate analyses data [41] for the rice husk samples are listed in **Table 1**, which could be used to characterize the composition of biomass, grasping its reaction characteristics and application value (*M*: moisture, *A*: ash, *V*: volatile, *FC*: fixed carbon; *C*: carbon, *H*: hydrogen, *O*: oxygen, *N*: nitrogen, *S*: sulfur).

The H-form rice husk was used as the raw material to supply real biomass tar. The raw pyrolysis biochar was mixed with an aqueous solution of 0.2 M H_2SO_4 in an acid solution:sample mass ratio of 30:1 and stirred in an argon atmosphere for 24 h. The slurry was filtered and washed with deionized water until the filtrate pH was constant (pH ≈ 7). After drying, the acid-washed sample is termed as the H-form char.

2.2 Biochar catalyst preparation

Pyrolysis biochar was used as the catalyst for biomass tar reforming. The set-up to pyrolysis biochar comprises a quartz reactor and a standard muffle furnace, as shown in **Figure 1**.

The quartz tray (red tray) with 5.0 g raw rice husk was placed into the quartz reactor. Along with the reactor cover, the quartz reactor was placed into the muffle furnace. At room temperature, the air in the reactor was displaced by Ar at a rate of 2.0 L/min for 30 min. Pyrolysis was performed at a slow-heating rate of 10°C/min up to a final pyrolysis temperature of 700°C with 70 min. Thereafter, with the temperature of turn-off furnace back to room temperature, the door of the muffle furnace was opened, and the reaction quenched by removing the reactor from the furnace. Ar gas was passed continuously through the reactor to prevent oxidation during cooling. The pyrolyzed biochar was removed from the reactor and stored at 4°C. Ar gas is supplied through a gas pipe (400 mm, long) into the porous distributor (with a diameter of 120 mm) and fed from the bottom of the quartz reactor filling the entire reactor. The upper cover acts as a partial seal under the action of its own gravity; however, with increasing internal gas volume produced as a function

Sample	Proximate analysis (wt.%)				Ultimate analysis (wt.%)				
	$M_{ad.}$	$A_{ad.}$	$V_{ad.}$	$FC_{ad.}$	$C_{ad.}$	$H_{ad.}$	$O_{ad.(diff)}$	$N_{ad.}$	$S_{t,ad.}$
Rice husk	6.86	17.00	60.92	15.22	37.35	4.40	34.05	0.20	0.14

Note: diff. = by difference, ad. = air dry basis.

Table 1.
Proximate and ultimate analyses of rice husk samples.

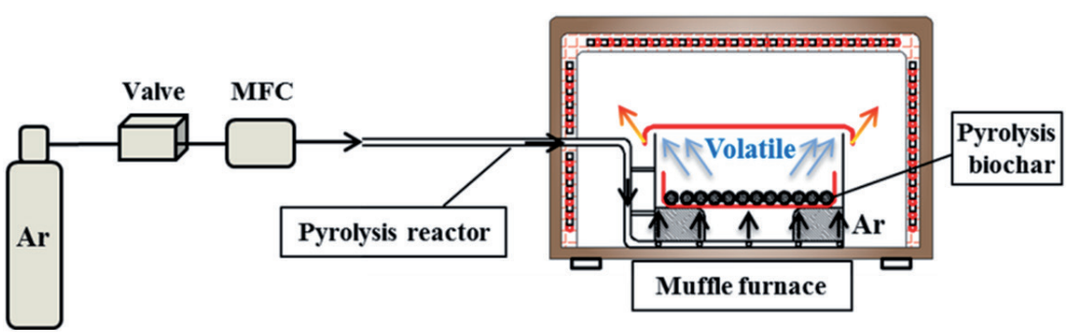

Figure 1.
Biochar catalyst preparation using a muffle furnace.

of muffle furnace temperature, some gaps between the upper cover and the reactor allow the release of gases under internal positive pressure. The volatile matters formed during the volatilization of biomass were rapidly dispersed away from the reactor, carried by Ar gas, so as to ensure an inert atmosphere inside the reactor. The metal contents of the origin and H-form biochar are listed in **Table 2**.

2.3 Homogeneous/heterogeneous reforming of biomass tar

As shown in **Figure 2**, a two-stage fluidized bed/fixed bed reactor was used for the investigation of the homogeneous conversion and heterogeneous reforming of biomass tar over biochar. The inner diameter of the reactor was 37 mm. The reactor is divided into two layers by four quartz frits. The upper layer is fixed bed, while the lower is fluidized bed. The heights of upper and lower layers are 30 and

Biochar	Primary metal contents (wt.%)					
	Na	K	Mg	Ca	Al	Fe
Origin biochar	0.03	1.44	0.09	0.14	0.03	0.05
H-form biochar	0.00	0.02	0.01	0.01	0.01	0.01

Table 2.
Primary metal contents of pyrolysis rice husk biochar samples.

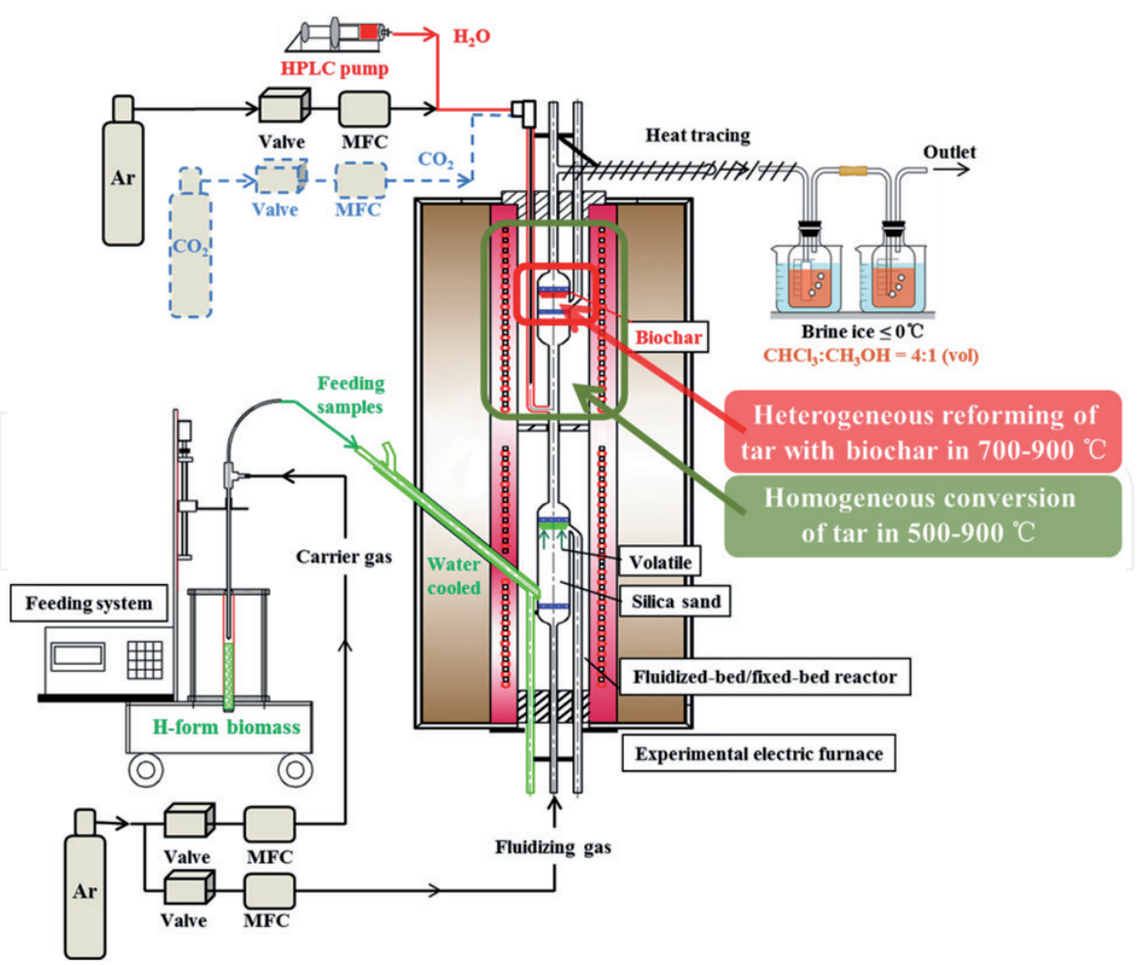

Figure 2.
Schematic diagram of a two-stage fluidized bed/fixed bed reactor for the homogeneous conversion and heterogeneous reforming of biomass tar.

130 mm, respectively. For the homogeneous conversion of tar, the lower fluidized bed reactor was heated to 500°C, with the temperature increased to 500–900°C for the upper fixed bed reactor (without catalyst). The silica sand with the weight of 60 g was pre-loaded into the bottom stage of the quartz reactor followed by Ar purging (1.0 L/min carrier gas and 1.5 L/min fluidizing gas) before heating the desired temperature. Once stabilization of the temperatures was achieved, the H-form rice husk was injected into the fluidized bed through the water-cooled pipes at a feeding rate of 100 mg/min. Simultaneously, for the CO_2 or H_2O separate treatment, the atmosphere was switched to CO_2 (29 vol.%) or H_2O (15 vol.%) through a dedicated gas injection system located in between the lower and upper reactors as shown in **Figure 2**. Pure Ar gas was also injected into the dedicated gas injection system, to balance the system, at rates of 1.03/0.92/0.82/0.75/0.68 L/min for reaction temperatures of 500/600/700/800/900°C, respectively, to maintain constant residence times for each reforming temperature. For 15 vol.% H_2O, steam injection was achieved by feeding a metered amount of water through a high-performance liquid chromatography (HPLC) pump into the heated zone of the reactor where the water was evaporated into steam. De-ionized H_2O was injected at rates of 0.34/0.30/0.28 ml/min along with 0.40/0.36/0.33 L/min of balanced Ar for the 700/800/900°C reaction temperatures, respectively. CO_2 was injected through the dedicated gas injection system at rates of 0.82/0.75/0.68 L/min to achieve 29 vol.% for 700/800/900°C reaction temperatures, respectively. The temperature was held for 10 min for each reaction. Reactions were terminated by switching the atmosphere to argon and removing the reactor out of the furnace.

For the heterogeneous reforming of biomass tar over biochar activated by H_2O or CO_2, the activation of biochar was carried out for 10 min in the fixed-bed zone in a 15 vol.% H_2O or a 29 vol.% CO_2 atmosphere with no supplemental H-form rice husk added to the fluidized-bed zone. This was followed by another 10 min at 800°C in an Ar atmosphere, to maintain the same total reaction time (20 min) as the tar-reforming conditions. Details of the five experimental conditions (A–E) are shown in **Table 3**. The experiments involved three pyrolysis experiments: tar reforming (A) in Ar with unactivated pyrolysis biochar; (B) in Ar over H_2O-activated biochar; and (C) in Ar over CO_2-activated biochar. In (B) and (C), a 10-min activation of the biochar was first carried out with the activated biochar then used for 10 min of tar reforming in an Ar atmosphere at 800°C, while H-form biomass was also fed to the reactor. In addition, two gasification experiments were carried out: tar reforming in (D) a 15 vol.% H_2O atmosphere over H_2O-activated biochar and in (E) a 29 vol.% CO_2 atmosphere over CO_2-activated biochar. In (D) and (E), both atmospheres were kept constant for 20 min even though the period was evenly divided into a biochar-activation stage, which was followed by tar reforming over biochar.

Conditions	No.	Conditions of biomass tar reforming over biochar at 800°C
Pyrolysis	A	Biomass tar reforming in Ar over pyrolysis biochar
	B	Biomass tar reforming in Ar over H_2O-activated biochar
	C	Biomass tar reforming in Ar over CO_2-activated biochar
Gasification	D	Biomass tar H_2O reforming over H_2O-activated biochar
	E	Biomass tar CO_2 reforming over CO_2-activated biochar

Table 3.
Experimental conditions investigated for tar reforming over biochar.

2.4 Sampling and analysis of biochar and tar

The biomass tar compounds were trapped in two gas bottles, connected in series, and filled with a mixture of HPLC-grade chloroform and methanol (4:1, v/v), as shown in **Figure 2**. The bottles were placed in a brine ice bath (≤0°C). After the reaction, the total solution was transferred to a 200 mL volumetric flask and made up to volume with a mixture of chloroform and methanol (4:1, v/v).

The tar yield was determined by evaporating the solvents and water at 35°C for 4 h. The tar is thus experimentally defined as the material soluble in the chloroform/methanol (4:1, v/v) solvent mixture not being evaporated (with the solvents) at 35°C within 4 h [24, 25, 42]. The residues in the solvents themselves (i.e., blank) and the biomass moisture content were considered in the tar yield calculation. The equation used for tar concentration in the solution is shown as follows Eq. (1):

$$C = \frac{C_2 - C_1}{1 - C_2} \tag{1}$$

where C is the concentration of tar; C_1 is the concentration of the mixed solution residue (blank experiment); and C_2 is the concentration of residue in tar solution.

The equation used to determine tar yield is shown as follows Eq. (2):

$$\text{Tar yield} = \frac{C \times M_{\text{Tar solution}}}{M_{\text{biomass}}} \tag{2}$$

where C is the concentration of tar in the solution; $M_{\text{Tar solution}}$ is the total mass of tar collected in the solution; and M_{biomass} is the feed quality of the H-form rice husk into the reactor.

The samples were analyzed using an Agilent Gas Chromatography Mass Spectrometer (GC-MS) instrument (6890 series GC with a 5973 MS detector) with a capillary column (DB-5 ms; length 30 m, internal diameter 0.25 mm, film thickness 0.5 μm). The sample solution (5 μL) was injected into the injection port, set at 260°C, with a split ratio of 80:1. The column was operated in constant-flow mode using 2.0 mL/min of helium as the carrier gas. The column temperature was initially maintained at 35°C for 3 min, then increased to 260°C at a heating rate of 10°C/min, and then maintained at 260°C for 5 min. Mass spectra were acquired after a 4-min solvent delay [21]. The chromatogram peaks were identified by comparison with the standard spectra of compounds in the National Institute of Standards and Technology library (NIST) and/or from the retention times/spectra of known injected species.

The total amount of metal species in the biochar samples was quantified by employing a previously established procedure [43]. Using a microwave system (Ethos 1, Milestone, Sorisole, Italy), the sample (0.1 g) was digested in a 1:3:8 (v/v/v) mixture of 40% HF, 30% H_2O_2, and 65% HNO_3 at 200°C for 60 min. The metal species content was then quantified by inductively coupled plasma-atomic emission spectroscopy (ICP-AES). Three measurements were conducted with the average values and then taken as the results.

The biochar's particle morphology and surface composition were measured by an EVO18 scanning electron microscope coupled to an energy dispersive X-ray spectrometer (SEM-EDX, Carl Zeiss, Germany).

Biochar samples were set for at least 24 h to displace the reaction gas within the pore structure with air. N_2-adsorption isotherms were then obtained at −196°C (ASAP 2020M, Micromeritics Instrument Crop, USA) and analyzed by the BET model to determine the sample's surface area and pore volume.

XPS analysis was used to evaluate the characteristics of surface elements in biochar. This was performed using a K-Alpha spectrometer (Thermo Fisher Scientific)

equipped with monochromatic Al Kα X-rays at 1486.6 eV. To exclude effects on the binding energies caused by changing the sample during measurements, the data were corrected by a linear shift with the maximum peak of the C1s binding energy of the adventitious carbon corresponding to 284.6 eV. The surface's elemental condition was analyzed using the number of escaped electrons from the char surface at a depth of 1–10 nm, according to the findings in our previous investigations [44, 45].

3. Results and discussion

3.1 Homogeneous conversion of biomass tar

The homogeneous conversion of tar mainly refers to the initial pyrolysis tar experiences during a series of decomposition and polymerization processes under ambient conditions (heat and atmosphere). Tar yield during the Ar, H_2O, and CO_2 homogeneous conversion experiments performed at 500–900°C can be seen in **Figure 3**. In the presence of an Ar-only atmosphere, the tar yield decreased gradually as a function of increasing temperature from 500 (26.18%) to 900°C (6.38%). Temperature in the Ar-only experiments has a greater influence between 500 and 700°C. Further increasing the temperature to 700–900°C results in increased biomass decomposition, thus lowering tar yields. Thermal decomposition is considered to be the main factor in the conversion of tar [46, 47]. As shown in **Figure 3**, in 15 vol.% H_2O and 29 vol.% CO_2, the effects of H_2O and CO_2 on the homogeneous transformation of biomass tar over biochar are significant. At the same temperature, the tar reforming effect of 15 vol.% H_2O is significantly higher than that of 29 vol.% CO_2. In 15 vol.% H_2O, the tar yield decreased from 6.95% at 700°C to 3.56% at 900°C. In 29 vol.% CO_2, the tar yield decreased from 7.99% at 700°C to 5.01% at 900°C. For the higher temperatures, 700–900°C are required for H_2O and CO_2 to influence tar homogeneous transformations, while for the lower temperatures, 500 and 600°C are not in the gasification thermal range.

As shown in **Figure 4**, it can be seen that at lower temperatures (500–600°C), the majority of the biomass tar still comprises components based on the primary biomass tar containing oxygen and substituent compounds, such as levoglucosan and dimethoxymethane. However, when subjecting the biomass to higher temperatures (700–900°C), most of the primary pyrolyzed tar gradually transforms [48]. The tar composition seems to be mainly composed of aromatic compounds having

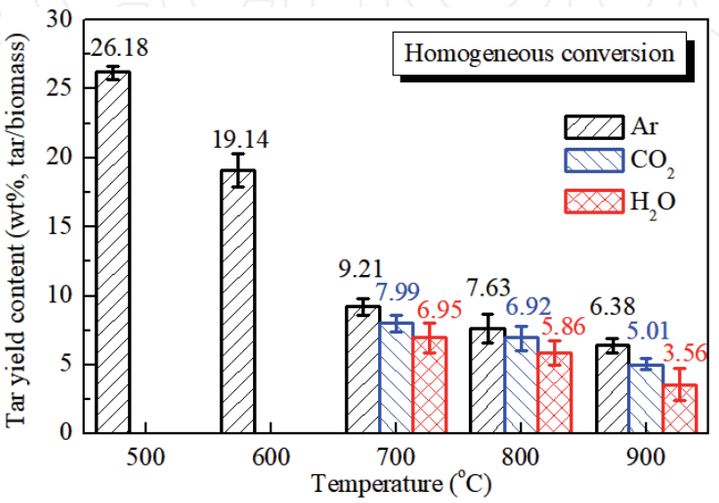

Figure 3.
Tar yield during homogeneous conversion at 500–900°C.

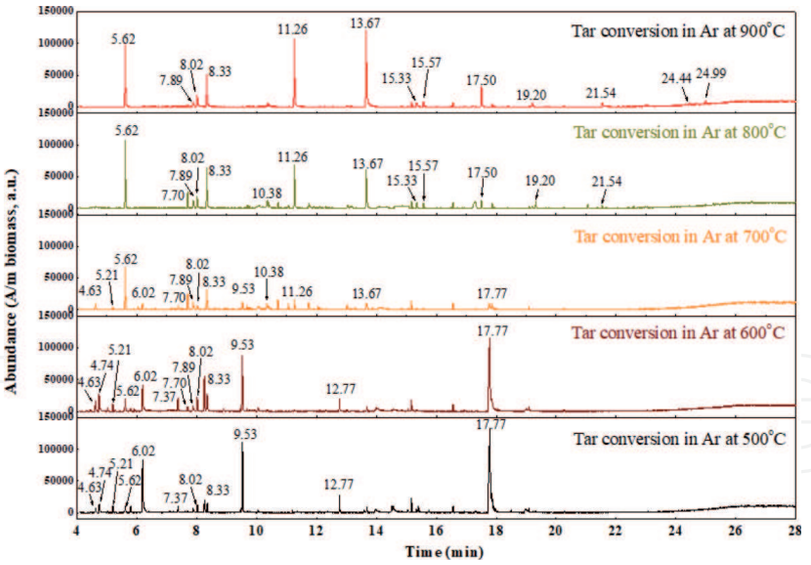

Figure 4.
GC-MS analysis of biomass tar in Ar at 500–900°C.

good thermal stability, such as toluene, indene, and naphthalene, among others. Increasing the temperature resulted in either a gradual reduction or a complete removal of tars containing branched or heteroatom compounds, and polycyclic aromatic hydrocarbons (PAHs) were gradually formed. For the biomass tar homogeneous conversion, the aromatic ring structure has higher thermal stability than that of the non-aromatic structures. Specific tar components decompose into small molecular gases and C_1–C_5 hydrocarbons, while there is evidence for the promotion of aromatic rings as a function of increasing temperature. H-abstraction, C_2H_2-addition (HACA), and cyclodehydrogenation are the mechanisms typically responsible for such processes [49, 50]. Performing the reactions at the mid-temperature range (700–800°C) results in aromatic conversion with oxygen and substituents. Thermal decomposition [51] and additional reactions convert short-chain hydrocarbons (C_1–C_5) into compounds containing unsaturated double and triple bonds that gradually increase in concentration by the acetylene addition reaction. The aromatic components can also be polymerized by dehydrogenation. Further increasing the temperature to 900°C results in the relative content of PAHs, such as naphthalene, phenanthrene, and anthracene, to increase the above conversion pathway yielding highly stable aromatic hydrocarbons.

GC-MS analysis during H_2O and CO_2 homogeneous conversion at 700–900°C can be seen in **Figure 5**. At 700–900°C, H_2O and CO_2 have a degree of influence on the conversion of tar. The degree of tar homogeneous conversion in the presence of either a H_2O or CO_2 atmosphere was significantly higher than that of the thermal decomposition in Ar. PAH concentration was low. The results show that H_2O and CO_2 have obvious effects on the transformation of aromatics, especially PAHs [52]. The free radical theory is used to explain the homogeneous transformation of tar. The formation of aromatic radicals in the polymerization of aromatic hydrocarbons is considered to be the key to the reaction. The continuous polymerization process is considered to be the main pathway [53–56]. Thermal decomposition is a method of generating free radicals through thermal breaking of bonds. The free radicals generated by the original tar form different final products by reacting with different free radicals produced as a function of the atmosphere. The presence of H_2O and CO_2 promoted the formation of free radicals with H/O/OH moieties. The influence of temperature is mainly reflected in the promotion of the decomposition reaction caused by free radicals [57]. CO_2 is a pure oxygen donor. **Figure 6** shows that the active oxygen atoms used for oxidative decomposition of hydrocarbons and intermediate

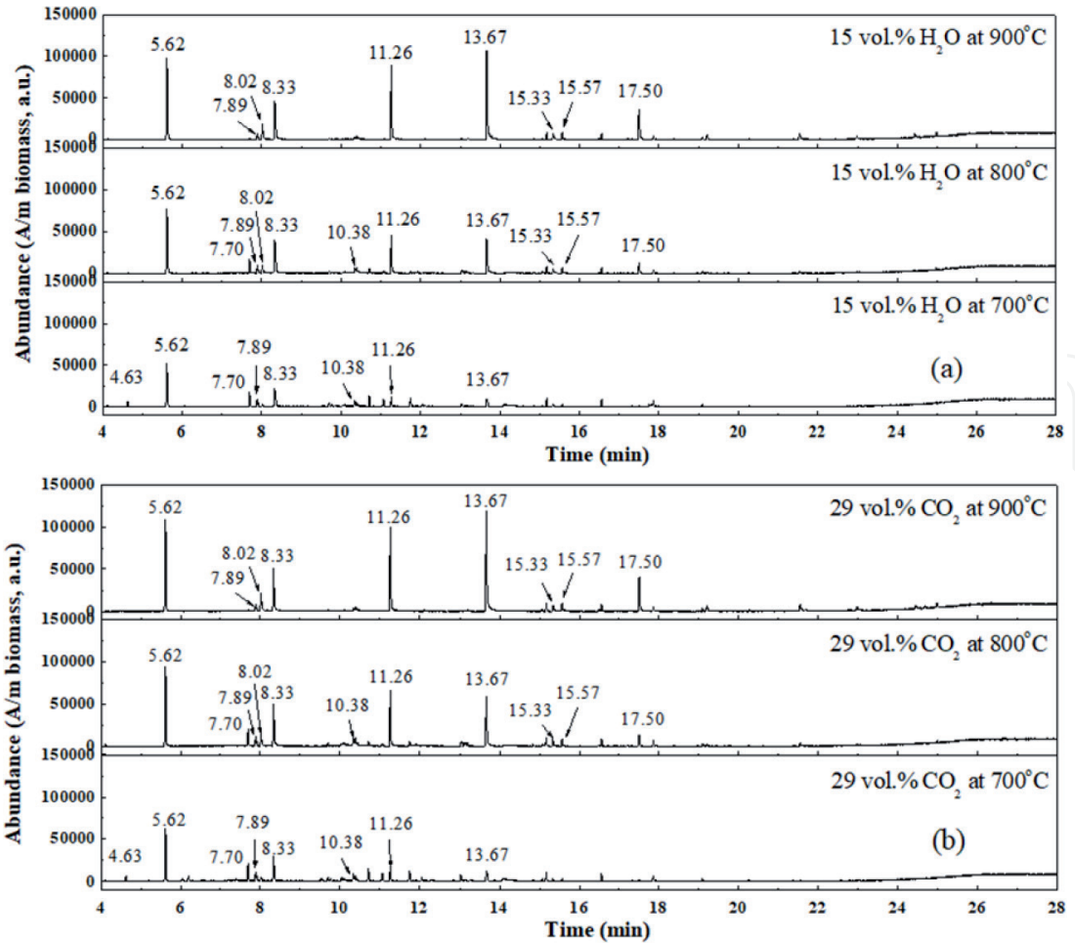

Figure 5.
GC-MS tar analysis during (a) 15 vol.% H_2O and (b) 29 vol.% CO_2 homogeneous conversion at 700–900°C.

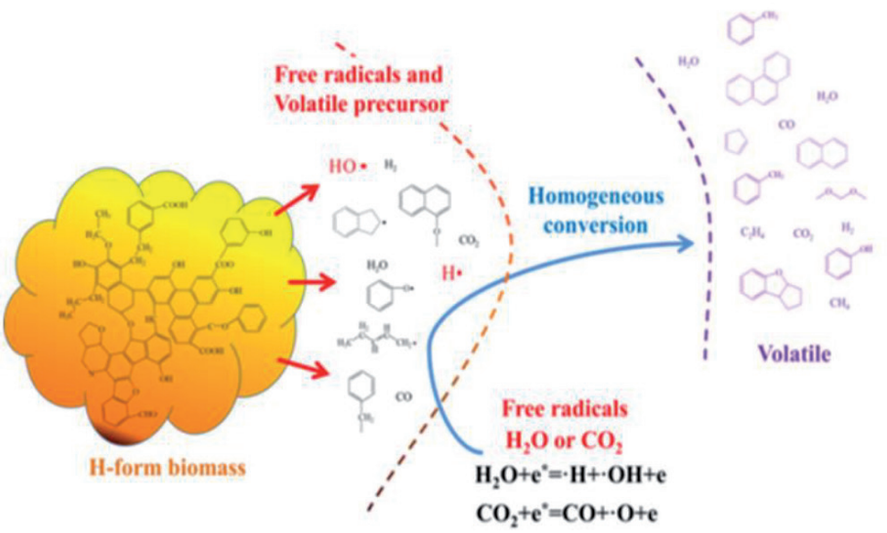

Figure 6.
Homogeneous conversion of tar in Ar, H_2O, and CO_2 at 500–900°C [52].

products are mainly produced by the reaction $CO_2 + e\times \rightarrow CO + O\cdot + e$. Active OH free radicals can be formed by replacing the hydrogen atoms in the hydrocarbons with oxygen atoms. Increasing the content of CO_2 is helpful to inhibit the cyclization of aromatics. The addition of CO_2 promotes the formation of free radicals such as O, which can further react with hydrocarbon groups. The oxidation reaction of active oxygen atoms with hydrocarbons forms CO, H_2O, and other products. The oxidative cracking process of tar is initiated, and the polymerization process of aromatic

hydrocarbons is also inhibited. H_2O not only promotes tar cracking conversion but also inhibits the polymerization reaction. This is related to the higher activity of free radical formation being a more active reformer in the conversion of tar. H_2O and CO_2 have similar oxidation capacities. The difference between the two is mainly reflected in the product—H_2O produces higher numbers of H free radicals than CO_2 [58]. O and OH free radicals can be formed by ionization of H_2O ($H_2O \rightarrow H + OH$) in the presence of steam. The fracture of OH can form new H and O free radicals. The H/O/OH atoms in the gas phase exist in radical form. According to the free radical mechanism, the primary constituents of the biomass are broken into activated tar fragments at high temperatures. A large number of H/O/OH free radicals will combine with activated tar fragments before tar polymerization.

As shown in **Figure 6**, the conversion of the tar homogeneous transformation process is considered to be a two-stage process. The first stage involves the decomposition and transformation of the active heteroatom-containing groups in the tar, along with the decomposition of dealkylated side chains, hydrocarbon molecular cyclization, and aromatization reactions. The products include low-chain aliphatic hydrocarbons, oxygen-containing small molecular gases, and single-ring aromatic hydrocarbons. The second stage is the reforming of tar components; the dehydrogenation of cyclization products; the addition of acetylene; and the growth, recombination, and isomerization of aromatics. The two processes constitute the basis of the biomass tar homogeneous reaction. In the presence of different reforming agents (H_2O or CO_2), the atmosphere can promote or inhibit tar pyrolysis conversion, thus influencing the composition of the final tar. The addition of H_2O and CO_2 can promote the generation of active free radicals such as O, OH, H, and so on. These free radicals can react with the active free tar fragments generated from the first stage of thermal decomposition demonstrating the importance of the H_2O and CO_2 reforming agents in the homogeneous conversion of biomass tar.

3.2 Heterogeneous reforming of biomass tar over biochar

3.2.1 Biomass tar reforming

As shown in **Figure 7**, the highest proportion of bio-tar was reformed (including homogeneous and heterogeneous phases) in the 15 vol.% H_2O atmosphere over H_2O-activated biochar (D). The proportion of tar reformed in the 29 vol.% CO_2 atmosphere over CO_2-activated biochar (E) was also considerably higher than results for reforming in an Ar atmosphere (A, B, and C). This illustrates that the presence of a gasification agent (H_2O/CO_2) greatly promotes in-situ reforming of nascent bio-tar over biochar. Under pyrolysis conditions, the homogeneous transformation of biomass tar was mainly based on secondary reactions (i.e., tar thermal cracking at 800°C), yielding a conversion efficiency of 70.86%. The ability of H_2O/CO_2 activation to improve biochar reactivity was also clearly observed. In the Ar atmosphere, the highest proportion of tar was reformed over the H_2O-activated biochar (B, 20.08%), followed by that over the CO_2-activated biochar (C, 19.01%), while the lowest conversion was for the (unactivated) pyrolysis biochar (A, 17.41%). El-Rub and Kamel [59] and Chen et al. [60] studied biochar's catalytic activity for tar reforming using a fixed char bed. They concluded that in an inert atmosphere, the tar molecules were mainly adsorbed on biochar active sites and converted into larger polyaromatic molecules and coke via a series of dehydrogenation, cyclization, and condensation reactions. Differences between the unactivated and H_2O/CO_2-activated biochars may be attributed to differences in inherent catalytic AAEM species (such as K and Ca) and the biochars' physiochemical structures [61], as discussed later.

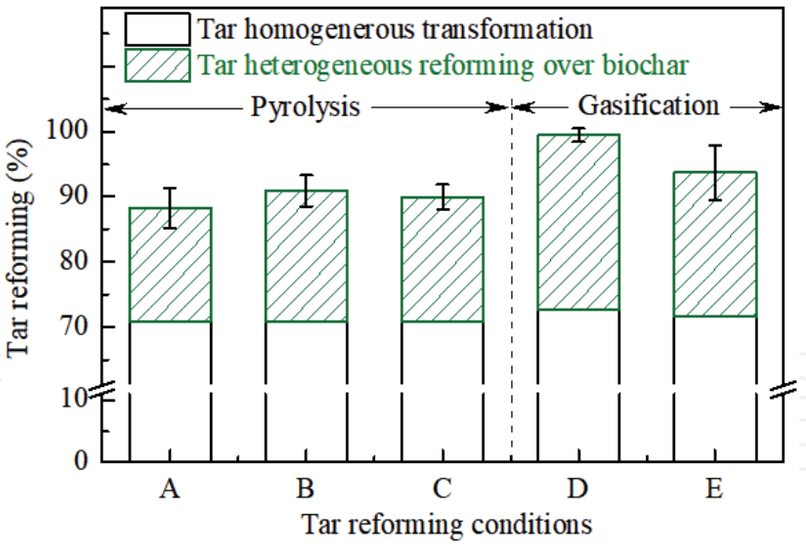

Figure 7.
Proportion of tar reformed under different conditions: (A) in Ar over pyrolysis biochar, (B) in Ar over H_2O-activated biochar, (C) in Ar over CO_2-activated biochar, (D) in 15 vol.% H_2O over H_2O-activated biochar, and (E) in 29 vol.% CO_2 over CO_2-activated biochar.

The presence of a gasification agent further improved the homogeneous reforming of the bio-tar (72.62 and 71.57% with H_2O and CO_2 present, respectively). The homogeneous transformation of biomass tar in the gas phase was in a certain extent in H_2O/CO_2 gasification condition, which was in broad agreement with the results obtained by Wang et al. [17] and Min et al. [24]. Besides, in the gasification conditions, H_2O and CO_2 further improved the biochar's catalytic reactivity for the heterogeneous reforming process with the proportion reformed increasing from 20.08% (B) to 26.85% (D) with H_2O and from 19.01% (C) to 22.17% (E) with CO_2. According to Min et al. [24], the reforming of tar molecules over biochar may be activated in two ways. First, in the gas phase, nascent tar (volatiles) contains abundant free radicals that would react with extant tar molecules to form activated tar fragments. Second, tar molecules and biochar may be activated by H_2O/CO_2 during the chemisorption of tar on the biochar surface with reactions between tar and H_2O/CO_2 adsorbed on the biochar's active sites then leading to further reforming reactions. Overall, gasification agents (H_2O and CO_2) improved and maintained the system's ability to carry out homogeneous and heterogeneous reforming of biomass tar.

3.2.2 H_2O/CO_2 activation of biochar

The metal contents of the biochar samples are shown in **Table 4**. Apart from K, there was little difference (±0.02 wt.%) observed for the metals between the biochar samples. During the H_2O/CO_2 activation of biochar, K appears to have been released from the biochar, decreasing from 1.12 wt.% in the pyrolysis biochar to 1.06 wt.% when activated by H_2O and 1.09 wt.% in the CO_2-activated biochar.

Biochar samples	**Metal species content (wt.% in biochar)**				
	K	**Mg**	**Ca**	**Fe**	**Al**
H_2O-activated biochar	1.06	0.10	0.16	0.06	0.02
CO_2-activated biochar	1.09	0.09	0.15	0.05	0.03

Table 4.
Biochar samples' metal-content analysis.

Because of their valence states [43], other metal species like Ca bond to the biochar more strongly (i.e., at two or more sites) than K (which only bonds at one site).

3.2.3 SEM-EDX analysis of biochar

As shown in **Figure 8(a)**, the unactivated biochar particles' surfaces showed more, larger (40 × 60 μm) hill-like structures than the surfaces of the activated biochars. H_2O and CO_2 activate the biochar via $C + H_2O \rightarrow CO + H_2$ and $C + CO_2 \rightarrow 2CO$, respectively. However, its larger size meant activation by CO_2 was limited to the surface of biochar, resulting in small structures (15 × 15 μm), which can be seen in **Figure 8(c)**. However, as illustrated by the structure shown in **Figure 8(b)**, H_2O, as well as H/O/OH radicals, was able to alter the surface morphology (creating structures of 20 × 20 μm) and infiltrate into the particle's carbon matrix to produce new larger pore structures from the inside out. According to Wu et al. [62], interactions between radicals and metal species take place on the surface of internal pores or inside the char matrix. **Table 4** shows little change in the biochar's internal metal (K, Ca, Mg, Fe, and Al) contents before and after H_2O/CO_2 activation. Thus, the effect of H_2O/CO_2 may be more focused on changing the distribution of metal species within the biochar samples. As we reported previously [43], the effect of K in biochar on tar reforming is stronger than that of Ca and other species. Thus, the surface content and distribution of K were studied, as shown in **Figure 8(a)–(c)**. The surface content of K significantly increased from 0.18% in the unactivated biochar to 0.35% in the H_2O-activated biochar and 0.21% in CO_2-activated biochar. In addition, an obvious enrichment occurred on the surface of H_2O-activated biochar. Klinghoffer et al. [63] reported that during thermal treatment the metal species migrated to the biochar surface, some of which formed clusters that then acted as an active site for catalytic reactions. During H_2O/CO_2 activation, an increase in surface O content occurred alongside the migration of AAEM species from the interior of the particles to the surface, forming metal-carbon complexes. The redox properties of these metal-carbon complexes may have had implications for the biochar's catalytic properties. Also, highly dispersed metal species in a highly porous carbon matrix could have effectively acted as active adsorption sites that

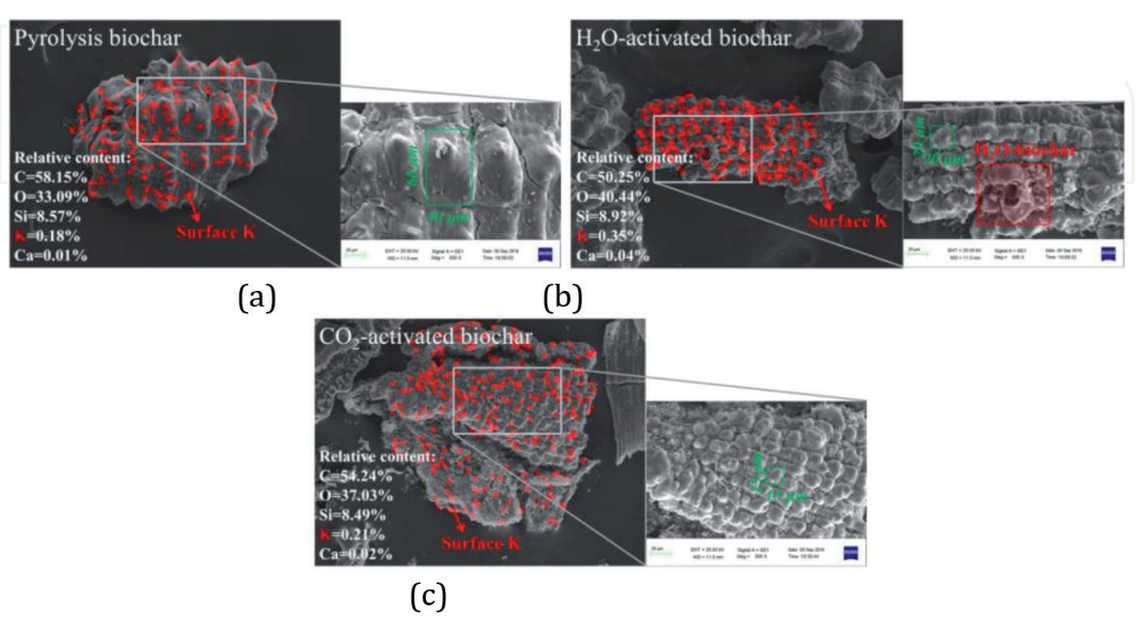

Figure 8.
SEM-EDX analysis of biochar samples. (a) Pyrolysis biochar, (b) H_2O activated biochar, and (c) CO_2 activated biochar.

promote volatile hydrocarbon condensation reactions to form coke [25], which were caused by hydrodeasphalting (HDA) reactions. Thus, the H_2O/CO_2 activation of biochar impacted the biochar surface's morphology and metal content, both of which influenced the reforming of biomass tar over biochar.

3.2.4 BET analysis of biochar during H_2O/CO_2 activation and tar reforming

The biochar samples' N_2-absorption/desorption isotherms at 77 K during H_2O/CO_2 activation and biomass tar reforming are shown in **Figure 9**. Compared with those of the original pyrolysis biochar, the pore systems of H_2O/CO_2-activated biochar samples and that from tar H_2O reforming over H_2O-activated biochar were better developed. Conversely, the other conditions exhibited pore structures that were somewhat blocked, especially for reforming over pyrolysis biochar in Ar and for the CO_2-activated biochar.

To further investigate the microphysical structures of the biochar samples, their BET surface properties were evaluated and are presented in **Table 4**. The unactivated pyrolysis biochar presented a BET surface area of 195.35 m^2/g and a pore volume of 0.0999 cm^3/g. Activation by H_2O and CO_2 increased the BET surface area to 307.45 and 237.71 m^2/g, respectively. The biochar's porous structure enabled efficient tar adsorption, resulting in a good residence time of the tar reacting with the catalyst [46]. **Table 5** also shows that the concentration of micropores (<2 nm), mesopores (2–50 nm), and macropores (>50 nm) varied between the samples. Thus, the ratio of micropores (<2 nm) to mesopores and macropores (>2 nm) ($S_{Mic.}/S_{Ext.}$) was employed. The H_2O-activated biochar showed a lower value of this ratio (2.28) than that of the CO_2-activated biochar (4.57) indicating that activation/gasification under a CO_2 atmosphere produced a higher relative micropore content, whereas under an H_2O atmosphere mesopores were favored. This may be explained by considering that H_2O removes carbon atoms from the particle's interior, enlarging open micropores and opening closed micropores, promoting the formation of mesopores. Meanwhile, CO_2 causes changes in the biochar surface that create more micropores. According to Klinghoffer et al. [63], the higher biochar surface area was the main reason for better catalyst performance, but pore size distribution also affected its activity, and evidence of diffusion limitations in microporous biochar was observed. Elsewhere, it has been confirmed that mesopores significantly

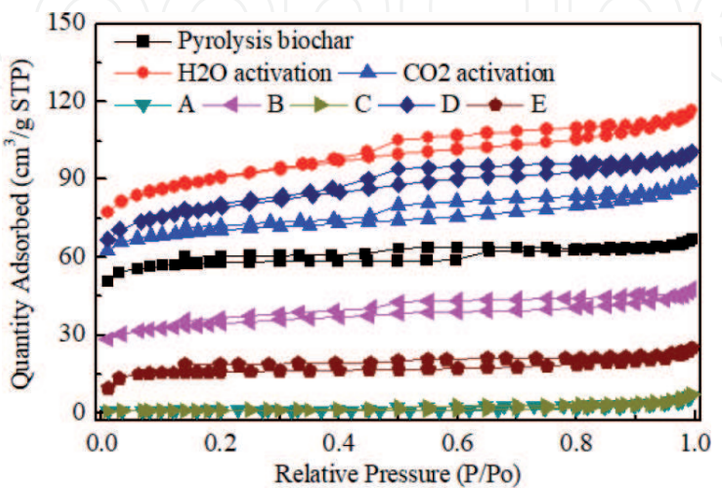

Figure 9.
N_2-absorption/desorption isotherms at 77 K for biochar obtained from different conditions: (A) in Ar over pyrolysis biochar; (B) in Ar over H_2O-activated biochar; (C) in Ar over CO_2-activated biochar; (D) in 15 vol.% H_2O over H_2O-activated biochar; and (E) in 29 vol.% CO_2 over CO_2-activated biochar.

enhance catalytic activity by allowing the penetration of macromolecules, facilitating their adsorption on the catalyst surface [64–66]. Thus, biochar used for catalytic tar reforming should ideally possess a high surface area and high mesoporosity (i.e., a small $S_{Mic.}/S_{Ext.}$ value).

After tar reforming in the Ar atmosphere, the biochar samples' BET surface area and pore volume markedly decreased. This was especially the case for tar reforming in Ar over the pyrolysis biochar and the CO_2-activated biochar where the BET surface areas fell to 3.78 and 4.07 m_2/g, respectively. According to the findings of Hosokai et al. [19], the decrease in surface area was attributed to tar forming coke deposits on the biochar's surface. In the Ar atmosphere, tar was mainly decomposed via coking [C_mH_n (aromatic compounds) = C_mH_x(coke) + $(n-x)/2\ H_2$]. Thus, the biochar's activity could have fallen with a decrease in the biochar's surface area and/or pore volume caused by coke deposition. This implies that when some tar molecules reacted with the biochar they were absorbed in a way that yielded a condensed-phase product (coke) that remained on the biochar surface.

However, with the gasification agents, especially H_2O, the relatively high BET surface area and pore volume of biochar were maintained following the tar-reforming reactions (see **Table 5**). This indicated that the tar was not reformed directly to give gaseous products but instead involved the intermediate formation of coke, which was subsequently gasified by H_2O/CO_2. El-Rub and Kamel [59] suggested that tars can be adsorbed onto the active sites of biochar particles. Adsorbed tar and coke molecules can be catalytically reformed to give CO and H_2 by steam and dry CO_2 thermochemical reactions, regenerating the pore structure. Meanwhile, free radicals that enter polymerization reactions and coke on biochar surfaces can be formed from tar decomposition. For the H_2O-activated biochar, the BET surface area only decreased a little following reforming (to 268.52 m^2/g) and the $S_{Mic.}/S_{Ext.}$ value remained 2.30. Given that these conditions also reformed the greatest portion of the tar, the existence of gasification agents, especially H_2O, appeared to stimulate and maintain catalytic activity by continually creating and regenerating pore structures in the biochar.

Conditions	BET surface area	Pore volume	Micro pore < 2 nm	External pore > 2 nm	$S_{Mic.}/S_{Ext.}$
	(m^2/g)	(cm^3/g)	(m^2/g)	(m^2/g)	
Pyrolysis biochar	195.35	0.0999	170.46	24.89	6.85
H_2O-activated biochar	307.45	0.1745	213.83	93.62	2.28
CO_2-activated biochar	237.71	0.1330	195.02	42.69	4.57
(A) Pyrolysis and Ar reforming	3.78	0.0070	3.14	0.65	4.86
(B) H_2O activation and Ar reforming	117.53	0.0693	78.28	39.25	1.99
(C) CO_2 activation and Ar reforming	4.07	0.0074	2.12	1.95	1.09
(D) H_2O activation and H_2O reforming	268.52	0.1512	187.08	81.44	2.30
(E) CO_2 activation and CO_2 reforming	54.31	0.0346	42.98	11.33	3.79

Table 5.
BET properties of biochar samples during activation and tar reforming.

3.2.5 XPS analysis of biochar during biomass tar reforming

The elemental contents (C, O, K, and Ca) at the surface of the biochar samples are shown in **Figure 10**. Samples taken the following tar reforming in (A) Ar over pyrolysis biochar, (B) Ar over H_2O-activated biochar, and (C) Ar over CO_2-activated biochar showed that the H_2O/CO_2 activation of biochar played an important role in maintaining the biochar's active sites, such as surface O-containing functional groups and AAEM species (especially K and Ca) and improved its tar-reforming performance. According to Du et al. [67], XPS revealed the evolution of AAEM species and char structures, and concentrations of AAEM species agreed well with surface atomic O concentrations. Similar results were obtained in **Figure 10**, where Ar reforming over H_2O-activated biochar yielded a biochar with a higher surface content of O (16.25 atomic%), K (0.80 atomic%), and Ca (0.45 atomic%) than the samples from Ar reforming with the CO_2-activated biochar and the pyrolysis biochar. Abundant O-containing groups on the biochar surface can form acidic centers that can combine with biomass tar precursors, which have negatively charged π-electron systems and activate thermal cracking reactions [61]. For tar reforming in Ar, more carboxylic (O=C–O)/carbonyl (C=O) groups and fewer aromatic (C–C/C=C) groups were formed on the H_2O/CO_2-activated biochar surface. Franz et al. [68] investigated the effects of O-containing groups, particularly carboxylic and carbonyl groups, on the adsorption of dissolved aromatics on ash-free activated carbon. They found that the adsorption mechanism was influenced by the surface functional group's properties, especially its ability to hydrogen-bond, and through its activating/deactivating influence on the tar's aromatic ring. As shown in **Figure 5** for conditions (D) and (E), the existence of the gasification agents during tar reforming over H_2O/CO_2-activated biochar helped to limit coke formation on the biochar surface, likely by continually creating and regenerating surface active sites. This finding was consistent with that of a previous investigation [24].

The surface AAEM content remained high. For example, 2.12 atomic% K in H_2O and 1.83 atomic% in CO_2. This was similar for the surface O content (34.01 atomic% in H_2O and 32.07 atomic% in CO_2). A biochar with a higher O content appeared to favor the retention of AAEM species, with O likely serving as a link between the AAEM species and the char matrix [69]. In addition, the results of Wu et al. [70] suggest that adding H_2O was likely to have eliminated more tar, while the presence of CO_2 induced the formation of OH, H, and O radicals, which increase hydrocarbon conversion.

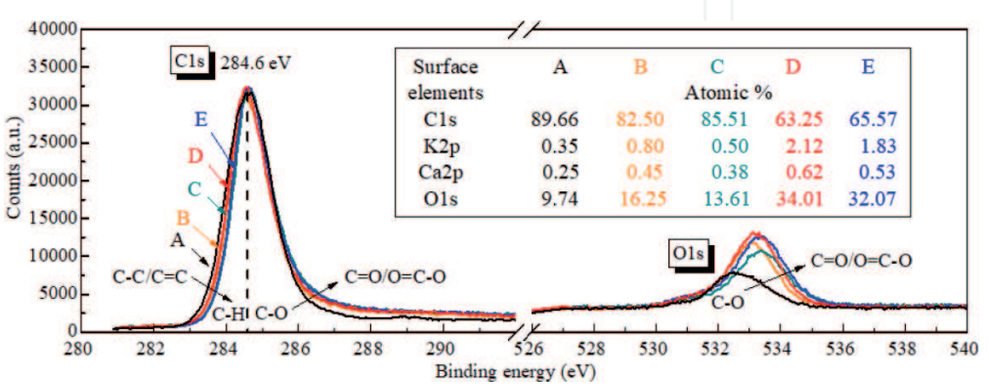

Surface elements	A	B	C	D	E
	Atomic %				
C1s	89.66	82.50	85.51	63.25	65.57
K2p	0.35	0.80	0.50	2.12	1.83
Ca2p	0.25	0.45	0.38	0.62	0.53
O1s	9.74	16.25	13.61	34.01	32.07

Figure 10.
XPS analysis of biochar samples from different conditions: (A) in Ar over pyrolysis biochar; (B) in Ar over H_2O-activated biochar; (C) in Ar over CO_2-activated biochar; (D) in 15 vol.% H_2O over H_2O-activated biochar; and (E) in 29 vol.% CO_2 over CO_2-activated biochar.

3.2.6 GC-MS analysis of biomass tar reforming over biochar

The biomass tar reformed in the gas phase (without involving biochar) in Ar at 800°C was mainly composed of aromatic tar compounds, owing to the secondary thermal cracking of in-situ biomass tar [52], compared with tar from H-form rice husk pyrolysis in fluidized bed at 500°C. Thermal cracking cannot completely convert tars [71]. Regarding the biochar catalyzed reactions, defined as the net tar loss owing to exposure to the biochar (i.e., the amount remaining after subtracting the amount of tar destroyed by vapor-phase cracking upstream and downstream of the biochar bed from the total change in tar amount during thermal treatment) [16], no new tar compounds were observed. According to Yao et al. [72], absent biochar, the gasification agent has a larger effect on the reforming of large aromatic ring systems (e.g., ≥2 fused benzene rings) than on smaller and isolated aromatics. However, here, biomass tars with a single aromatic ring or more than one ring structure were catalytically reformed over the various biochars. The conversion rates of tar compounds for the tar reformed without biochar in Ar at 800°C can be seen in **Figure 11(a)** and **(b)**. These figures also show that H_2O/CO_2 notably enhanced in-situ reforming of both large and small aromatic ring systems in biomass tar. For the experiments in Ar (conditions (A), (B), and (C)), individual tar conversion rates were improved by activation by H_2O/CO_2. For example, phenylethyne conversion increased from 42.27% over pyrolysis biochar to 77.43% over H_2O-activated biochar and to 49.93% over CO_2-activated biochar. However, the magnitude of the improvement was limited because of coke formation on the active sites, which deactivated the biochar. Thus, continuously supplying gasification agents (H_2O and CO_2 in conditions D and E, respectively) made more complete biomass tar conversion possible. For example, reforming in 15 vol.% H_2O over H_2O-activated biochar saw conversion rates of tars with both single aromatic ring structures (e.g., phenylethyne and benzofuran) and multiring structures (e.g., 1-methy-naphthalene, 2-methy-naphthalene, and phenanthrene) reach almost 100%. Although tar conversion was not completed in the 29 vol.% CO_2 atmosphere, it was also notably higher than for reforming in Ar over CO_2-activated biochar. As mentioned above, the gasification agent directly affected gas-phase tar reforming reactions [72], and it is likely that H_2O/CO_2 indirectly affected tar destruction by influencing the biochar structure and distribution of AAEM catalysts during the reaction by helping to ensure enough active sites on the biochar surface to maintain its catalytic activity.

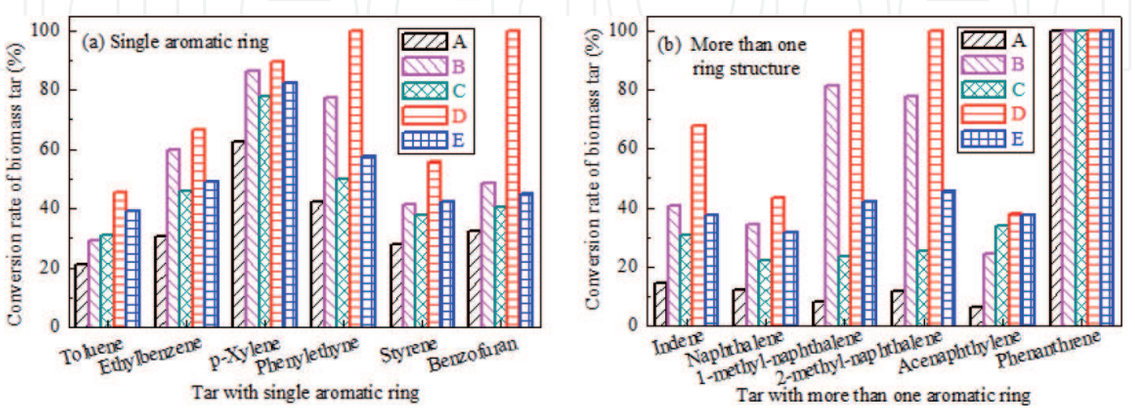

Figure 11.
Biomass tar conversion rates (based on tar observed following the treatment without biochar in Ar at 800°C) for different reforming conditions: (A) in Ar over pyrolysis biochar; (B) in Ar over H_2O-activated biochar; (C) in Ar over CO_2-activated biochar; (D) in 15 vol.% H_2O over H_2O-activated biochar; and (E) in 29 vol.% CO_2 over CO_2-activated biochar.

The heterogeneous reforming mechanism of the biomass tar over biochar and in the presence of the H_2O and CO_2 reforming agents at 800°C is shown in **Figure 12**. H_2O and CO_2 dissociate in space to form a large number of H/O/OH radicals, which play an important role in the tar-biochar reforming reaction. Biomass tar, through the biochar layer, is adsorbed onto the acid-base active sites (oxygen-containing functional groups and AAEM catalysts). The attraction effect of the carbon-rich biochar matrix invokes an electron pair shift in the tar molecules (relatively small mass), which promotes the tar molecules to break at high temperatures. According to the free radical theory [73], the tar adsorbed on the catalyst surface will catalytically crack to form the corresponding free radicals. The chemical reaction between these free radicals may permit new products. H_2O and CO_2 act as the reforming agents in the biochar carbon matrix, resulting in the fragmentation of the smaller aromatic rings. The empty active sites, formed by bond cleavage, were gradually occupied by H/O/OH radicals, forming active groups such as O-containing functional groups. In the presence of H_2O and CO_2, a significant amount of H/O/OH radicals in the vicinity ingress into the biochar carbon structure. The catalytic elements, such as AAEM species migrate at different rates and transformation from the carbon matrix onto the gas-solid interface or the gas phase undergoes, as shown in **Figure 12**. As the AAEM species are bonded with the C element on the biochar surface by the O element [21], H_2O and CO_2 react with these C elements on the biochar surface resulting in AAEM-O bond cleavage followed by precipitation. The valence state of Ca results in a stronger bonding interaction with the biochar when compared with K. Additionally, Ca migration and precipitation are more difficult than K. When tar adsorbs then cleaves the AAEM-O bond and functional group bond on the biochar surface, an aromatic fragmented radical is formed when other free radicals are encountered. At the same time, active AAEM species in the vicinity will continue to occupy active sites on the tar fragment groups, thereby inhibiting their secondary polymerization. At the same time, the H/O/OH radicals are exchanged to the AAEM species, which increases the possibility for the reforming of tar macromolecules. After the reaction, gas and light tars (C_nH_y/CO/H_2) were formed, thus realizing the H_2O or CO_2 heterogeneous reforming of biomass tar over the biochar catalyst.

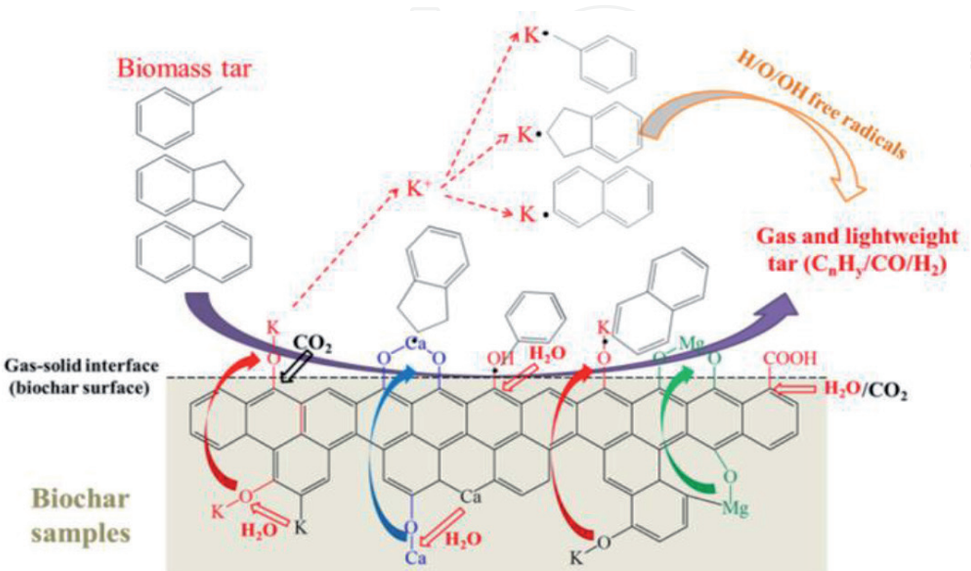

Figure 12.
Heterogeneous reforming mechanism of biomass tar over biochar in the presence of H_2O and CO_2 at 800°C [52].

4. Conclusions

The tar yield decreases as a function of increasing temperature from 26.18% at 500°C to 6.38% at 900°C. H_2O and CO_2 influence significantly the tar homogeneous transformations at 700–900°C, while the tar reforming effect of 15 vol.% H_2O is significantly higher than that of 29 vol.% CO_2. H_2O and CO_2 have obvious effects on the transformation of PAHs. H_2O and CO_2 not only directly affect the tar transformation on biochar but also indirectly influence the reforming of tar through changing the structure of biochar catalyst. The formation of additional oxygen-containing functional groups is strengthened with the concentration of H_2O and CO_2 increasing. During tar heterogeneous reforming over biochar, the transformation of small aromatic ring systems (3–5 fused rings) to larger aromatic ring systems (≥6 fused rings) in the biochar structure is promoted by the increasing concentration of H_2O and CO_2. The activation by H_2O/CO_2 of biochar impacted the biochar surface's morphology and distribution of metal species. Activation/gasification under a CO_2 in an Ar atmosphere produced more micropores, while adoption under a H_2O in an Ar atmosphere favored the formation of mesopores. With the existence of gasification agents, especially for H_2O, the simultaneous creation of pore structures is necessary to maintain biochar's catalytic activity during tar reforming. H_2O/CO_2 also indirectly affects tar destruction by influencing the biochar structure and distribution of AAEM catalysts, while the reaction is occurring to ensure enough active sites on the biochar surface to maintain its catalytic activity. The activation and/or activity-maintaining effects of H_2O/CO_2 can notably enhance the in-situ reforming of both large and small aromatic ring systems present in biomass tar.

Acknowledgements

This work is supported by the National Natural Science Foundation of China (51906052), the National Postdoctoral Program for Innovative Talents of China (BX20180086), China Postdoctoral Science Foundation Funded Project (2018M641826), Heilongjiang Provincial Postdoctoral Science Foundation, Foundation of State Key Laboratory of High-efficiency Utilization of Coal and Green Chemical Engineering (2019-KF-14), and Fundamental Research Funds for the Central Universities (Grant no. HIT. NSRIF. 2020052).

Conflict of interest

The authors declare no conflict of interest.

DOI: http://dx.doi.org/10.5772/intechopen.91380

Author details

Dongdong Feng*, Yu Zhang, Yijun Zhao and Shaozeng Sun
School of Energy Science and Engineering, Harbin Institute of Technology, Harbin, China

*Address all correspondence to: 08031175@163.com

References

[1] Shen Y, Zhao P, Shao Q, Ma D, Takahashi F, Yoshikawa K. In-situ catalytic conversion of tar using rice husk char-supported nickel-iron catalysts for biomass pyrolysis/gasification. Applied Catalysis B: Environmental. 2014;**152-153**:140-151

[2] Milne T, Evans R. Biomass gasification "tars": Their nature, formation and conversion. In: Report No. NREL/TP-570-25357. Golden, CO, USA: NREL; 1998

[3] Spath PL, Dayton DC. Preliminary screening-technical and economic assessment of synthesis gas to fuels and chemicals with emphasis on the potential for biomass-derived syngas. In: DTIC Document. 2003

[4] Bui T, Loof R, Bhattacharya S. Multi-stage reactor for thermal gasification of wood. Energy. 1994;**19**:397-404

[5] Mudge L, Baker E, Mitchell D, Brown M. Catalytic steam gasification of biomass for methanol and methane production. Journal of Solar Energy Engineering. 1985;**107**:88-92

[6] Kiel J, Van Paasen S, Neeft J, Devi L, Ptasinski K, Janssen F, et al. Primary measures to reduce tar formation in fluidised-bed biomass gasifiers. ECN, ECN-C-04-014. 2004

[7] Skoulou V, Kantarelis E, Arvelakis S, Yang W, Zabaniotou A. Effect of biomass leaching on H_2 production, ash and tar behavior during high temperature steam gasification (HTSG) process. International Journal of Hydrogen Energy. 2009;**34**:5666-5673

[8] Sarıoğlan A. Tar removal on dolomite and steam reforming catalyst: Benzene, toluene and xylene reforming. International Journal of Hydrogen Energy. 2012;**37**:8133-8142

[9] Dou B, Gao J, Sha X, Baek SW. Catalytic cracking of tar component from high-temperature fuel gas. Applied Thermal Engineering. 2003;**23**:2229-2239

[10] Rapagna S, Jand N, Foscolo P. Catalytic gasification of biomass to produce hydrogen rich gas. International Journal of Hydrogen Energy. 1998;**23**: 551-557

[11] Dayton D. A review of the literature on catalytic biomass tar destruction. US DOE NREL Report 510-32815. Golden, CO. 2002

[12] Abu El-Rub Z, Bramer E, Brem G. Review of catalysts for tar elimination in biomass gasification processes. Industrial & Engineering Chemistry Research. 2004;**43**:6911-6919

[13] Yu J, Tian F-J, McKenzie L, Li C-Z. Char-supported nano iron catalyst for water-gas-shift reaction: Hydrogen production from coal/biomass gasification. Process Safety and Environmental Protection. 2006;**84**:125-130

[14] Griffith DM, Mainhood J. Cracking of tar vapour and aromatic compounds on activated carbon. Fuel. 1967;**46**:167

[15] Chembukulam SK, Dandge AS, Rao NLK, Seshagiri K, Vaidyeswaran R. Smokeless fuel from carbonized sawdust. Industrial & Engineering Chemistry Product Research and Development. 1981;**20**:714-719

[16] Boroson ML, Howard JB, Longwell JP, Peters WA. Heterogeneous cracking of wood pyrolysis tars over fresh wood char surfaces. Energy Fuels. 1989;**3**:735-740

[17] Wang D, Yuan W, Ji W. Char and char-supported nickel catalysts for secondary syngas cleanup and

conditioning. Applied Energy. 2011;**88**:1656-1663

[18] Sueyasu T, Oike T, Mori A, Kudo S, Norinaga K, Hayashi J-i. Simultaneous steam reforming of tar and steam gasification of char from the pyrolysis of potassium-loaded woody biomass. Energy Fuels. 2011;**26**:199-208

[19] Hosokai S, Kumabe K, Ohshita M, Norinaga K, Li C-Z, Hayashi J-i. Mechanism of decomposition of aromatics over charcoal and necessary condition for maintaining its activity. Fuel. 2008;**87**:2914-2922

[20] Matsuhara T, Hosokai S, Norinaga K, Matsuoka K, Li C-Z, Hayashi J-i. In-situ reforming of tar from the rapid pyrolysis of a brown coal over char. Energy Fuels. 2009;**24**:76-83

[21] Feng D, Zhao Y, Zhang Y, Sun S, Meng S, Guo Y, et al. Effects of K and Ca on reforming of model tar compounds with pyrolysis biochars under H_2O or CO_2. Chemical Engineering Journal. 2016;**306**:422-432

[22] Yue B, Wang X, Ai X, Yang J, Li L, Lu X, et al. Catalytic reforming of model tar compounds from hot coke oven gas with low steam/carbon ratio over Ni/MgO-Al_2O_3 catalysts. Fuel Processing Technology. 2010;**91**:1098-1104

[23] Devi L, Ptasinski KJ, Janssen FJ. Pretreated olivine as tar removal catalyst for biomass gasifiers: Investigation using naphthalene as model biomass tar. Fuel Processing Technology. 2005;**86**:707-730

[24] Min Z, Asadullah M, Yimsiri P, Zhang S, Wu H, Li C-Z. Catalytic reforming of tar during gasification. Part I. Steam reforming of biomass tar using ilmenite as a catalyst. Fuel. 2011;**90**:1847-1854

[25] Min Z, Yimsiri P, Asadullah M, Zhang S, Li C-Z. Catalytic reforming of tar during gasification. Part II. Char as a catalyst or as a catalyst support for tar reforming. Fuel. 2011;**90**:2545-2552

[26] Sathe C, Pang Y, Li C-Z. Effects of heating rate and ion-exchangeable cations on the pyrolysis yields from a Victorian brown coal. Energy Fuels. 1999;**13**:748-755

[27] Li C-Z, Sathe C, Kershaw J, Pang Y. Fates and roles of alkali and alkaline earth metals during the pyrolysis of a Victorian brown coal. Fuel. 2000;**79**: 427-438

[28] Morf P, Hasler P, Nussbaumer T. Mechanisms and kinetics of homogeneous secondary reactions of tar from continuous pyrolysis of wood chips. Fuel. 2002;**81**:843-853

[29] Stiles HN, Kandiyoti R. Secondary reactions of flash pyrolysis tars measured in a fluidized bed pyrolysis reactor with some novel design features. Fuel. 1989;**68**:275-282

[30] Jess A. Mechanisms and kinetics of thermal reactions of aromatic hydrocarbons from pyrolysis of solid fuels. Fuel. 1996;**75**:1441-1448

[31] Li C-Z, Nelson PF. Fate of aromatic ring systems during thermal cracking of tars in a fluidized-bed reactor. Energy Fuels. 1996;**10**:1083-1090

[32] Williams PT, Taylor DT. Aromatization of tyre pyrolysis oil to yield polycyclic aromatic hydrocarbons. Fuel. 1993;**72**:1469-1474

[33] Kong M, Yang Q, Fei J, Zheng X. Experimental study of Ni/MgO catalyst in carbon dioxide reforming of toluene, a model compound of tar from biomass gasification. International Journal of Hydrogen Energy. 2012;**37**:13355-13364

[34] Takahashi H, Iwatsuki M, Essaki K, Tsutsumi A, Chiba T. Rapid conversion

of tar and char from pyrolysis of a brown coal by reactions with steam in a drop-tube reactor. Fuel. 2000;**79**:439-447

[35] Gil J, Corella J, Aznar MAP, Caballero MA. Biomass gasification in atmospheric and bubbling fluidized bed: Effect of the type of gasifying agent on the product distribution. Biomass Bioenergy. 1999;**17**:389-403

[36] Jönsson O. Thermal cracking of tars and hydrocarbons by addition of steam and oxygen in the cracking zone. In: Fundamentals of Thermochemical Biomass Conversion. Springer; 1985. pp. 733-746

[37] Zhang Y, Kajitani S, Ashizawa M, Oki Y. Tar destruction and coke formation during rapid pyrolysis and gasification of biomass in a drop-tube furnace. Fuel. 2010;**89**:302-309

[38] Wang Y, Namioka T, Yoshikawa K. Effects of the reforming reagents and fuel species on tar reforming reaction. Bioresource Technology. 2009;**100**: 6610-6614

[39] Miura K, Kawase M, Nakagawa H, Ashida R, Nakai T, Ishikawa T. Conversion of tar in hot coke oven gas by pyrolysis and steam reforming. Journal of Chemical Engineering of Japan. 2003;**36**:735-741

[40] Dufour A, Girods P, Masson E, Rogaume Y, Zoulalian A. Synthesis gas production by biomass pyrolysis: Effect of reactor temperature on product distribution. International Journal of Hydrogen Energy. 2009;**34**:1726-1734

[41] Feng D, Zhang Y, Zhao Y, Sun S. Catalytic effects of ion-exchangeable K^+ and Ca^{2+} on rice husk pyrolysis behavior and its gas-liquid-solid product properties. Energy. 2018;**152**:166-177

[42] Keown DM, Li X, Hayashi J-i, Li C-Z. Characterization of the structural features of char from the pyrolysis of cane trash using Fourier transform-Raman spectroscopy. Energy Fuels. 2007;**21**:1816-1821

[43] Feng D, Zhao Y, Zhang Y, Sun S, Meng S, Guo Y, et al. Effects of K and Ca on reforming of model tar compounds with pyrolysis biochar under H_2O or CO_2. Chemical Engineering Journal. 2016;**306**:422-432

[44] Zhao Y, Feng D, Zhang Y, Tang W, Meng S, Guo Y, et al. Migration of alkali and alkaline earth metallic species and structure analysis of sawdust pyrolysis biochar. Korean Chemical Engineering Research. 2016;**54**:659-664

[45] Zhao Y, Feng D, Zhang Y, Huang Y, Sun S. Effect of pyrolysis temperature on char structure and chemical speciation of alkali and alkaline earth metallic species in biochar. Fuel Processing Technology. 2016;**141**:54-60

[46] Gilbert P, Ryu C, Sharifi V, Swithenbank J. Tar reduction in pyrolysis vapours from biomass over a hot char bed. Bioresource Technology. 2009;**100**:6045-6051

[47] Dufour A, Masson E, Girods P, Rogaume Y, Zoulalian A. Evolution of aromatic tar composition in relation to methane and ethylene from biomass pyrolysis-gasification. Energy Fuels. 2011;**25**:4182-4189

[48] Milne TA, Abatzoglou N, Evans RJ. Biomass Gasifier "Tars": Their Nature, Formation, and Conversion. Golden, CO: National Renewable Energy Laboratory; 1998

[49] Ledesma E, Kalish M, Nelson P, Wornat M, Mackie J. Formation and fate of PAH during the pyrolysis and fuel-rich combustion of coal primary tar. Fuel. 2000;**79**:1801-1814

[50] Dong G, Hüttinger K. Consideration of reaction mechanisms leading to

pyrolytic carbon of different textures. Carbon. 2002;**40**:2515-2528

[51] Guan Y, Luo S, Liu S, Xiao B, Cai L. Steam catalytic gasification of municipal solid waste for producing tar-free fuel gas. International Journal of Hydrogen Energy. 2009;**34**:9341-9346

[52] Feng D, Zhao Y, Zhang Y, Sun S. Effects of H_2O and CO_2 on the homogeneous conversion and heterogeneous reforming of biomass tar over biochar. International Journal of Hydrogen Energy. 2017;**42**:13070-13084

[53] Badger GM, Kimber RWL, Spotswood TM. Mode of formation of 3, 4-benzopyrene in human environment. Nature. 1960;**187**(4738):663-665

[54] Rybak W, Zembruski M, Smith I. Twenty-First Symposium (International) on Combustion. Munich, Germany: The Combustion Institute; 1986. p. 231

[55] Badger G. Pyrolysis of hydrocarbons. Progress in Physical Organic Chemistry. 1965;**3**:1

[56] Poutsma ML. A Review of Thermolysis Studies of Model Compounds Relevant to Processing of Coal. TN, USA: Oak Ridge National Lab; 1987

[57] Futamura S, Annadurai G. Plasma reforming of aliphatic hydrocarbons with CO_2. ITIA. 2005;**41**:1515-1521

[58] Futamura S, Kabashima H, Annadurai G. Roles of CO_2 and H_2O as oxidants in the plasma reforming of aliphatic hydrocarbons. Catalysis Today. 2006;**115**:211-216

[59] El-Rub ZA, Kamel Z. Biomass char as an in-situ catalyst for tar removal in gasification systems. Fuel. 1990;**69**(10):1219-1225

[60] Chen G-M, Zhang X-W, Mi Z-T. Effects of pressure on coke and formation of its precursors during catalytic cracking of toluene over USY catalyst. Journal of Fuel Chemistry and Technology. 2007;**35**:211-216

[61] Wang F-J, Zhang S, Chen Z-D, Liu C, Wang Y-G. Tar reforming using char as catalyst during pyrolysis and gasification of Shengli brown coal. Journal of Analytical and Applied Pyrolysis. 2014;**105**:269-275

[62] Wu H, Quyn DM, Li C-Z. Volatilisation and catalytic effects of alkali and alkaline earth metallic species during the pyrolysis and gasification of Victorian brown coal. Part III. The importance of the interactions between volatiles and char at high temperature. Fuel. 2002;**81**:1033-1039

[63] Klinghoffer NB, Castaldi MJ, Nzihou A. Catalyst properties and catalytic performance of char from biomass gasification. Industrial & Engineering Chemistry Research. 2012;**51**:13113-13122

[64] Kyotani T. Control of pore structure in carbon. Carbon. 2000;**38**:269-286

[65] Frackowiak E, Beguin F. Carbon materials for the electrochemical storage of energy in capacitors. Carbon. 2001;**39**:937-950

[66] Ariyadejwanich P, Tanthapanichakoon W, Nakagawa K, Mukai S, Tamon H. Preparation and characterization of mesoporous activated carbon from waste tires. Carbon. 2003;**41**:157-164

[67] Du C, Liu L, Qiu P. Importance of volatile AAEM species to char reactivity during volatile-char interactions. RSC Advances. 2017;**7**:10397-10406

[68] Franz M, Arafat HA, Pinto NG. Effect of chemical surface heterogeneity on the adsorption mechanism of dissolved aromatics on activated carbon. Carbon. 2000;**38**:1807-1819

[69] Hashimoto K, Miura K, Xu J-J, Watanabe A, Masukami H. Relation between the gasification rate of carbons supporting alkali metal salts and the amount of oxygen trapped by the metal. Fuel. 1986;**65**:489-494

[70] Wu W-g, Luo Y-h, Su Y, Zhang Y-l, Zhao S-h, Wang Y. Nascent biomass tar evolution properties under homogeneous/heterogeneous decomposition conditions in a two-stage reactor. Energy Fuels. 2011;**25**:5394-5406

[71] Anis S, Zainal ZA. Tar reduction in biomass producer gas via mechanical, catalytic and thermal methods: A review. Renewable and Sustainable Energy Reviews. 2011;**15**:2355-2377

[72] Song Y, Wang Y, Hu X, Xiang J, Hu S, Mourant D, et al. Effects of volatile-char interactions on in-situ destruction of nascent tar during the pyrolysis and gasification of biomass. Part II. Roles of steam. Fuel. 2015;**143**:555-562

[73] Howard J. Fundamentals of coal pyrolysis and hydropyrolysis. Chemistry of Coal Utilization. 1981;**2**:665-784